Weather and Climate Extremes 42 (2023) 100616

Contents lists available at ScienceDirect

Weather and Climate Extremes

journal homepage: www.elsevier.com/locate/wace

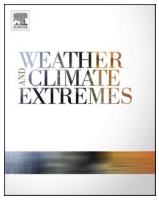

Human influences on spatially compounding flooding and heatwave events in China and future increasing risks

Cheng Qian [a,b,*], Yangbo Ye [a,b], Emanuele Bevacqua [c], Jakob Zscheischler [c,d]

[a] Key Laboratory of Regional Climate-Environment for Temperate East Asia, Institute of Atmospheric Physics, Chinese Academy of Sciences, Beijing, China
[b] University of Chinese Academy of Sciences, Beijing, China
[c] Department of Computational Hydrosystems, Helmholtz Centre for Environmental Research-UFZ, Leipzig, Germany
[d] Technische Universität Dresden, Dresden, Germany

ARTICLE INFO

Keywords:
Spatially compounding event
Extreme event attribution
Human contribution
Storyline approach
Risk-based approach
Carbon neutrality

ABSTRACT

Attribution of high-impact weather events to anthropogenic climate change is important for disentangling long-term trends from natural variability and estimating potential future impacts. Up to this point, most attribution studies have focused on univariate drivers, despite the fact that many impacts are related to multiple compounding weather and climate drivers. For instance, co-occurring climate extremes in neighbouring regions can lead to very large combined impacts. Yet, attribution of spatially compounding events with different hazards poses a great challenge. Here, we present a comprehensive framework for compound event attribution to disentangle the effects of natural variability and anthropogenic climate change on the event. Taking the 2020 spatially compounding heavy precipitation and heatwave event in China as a showcase, we find that the respective dynamic and thermodynamic contributions to the intensity of this event are 51% (35–67%) and 39% (18–59%), and anthropogenic climate change has increased the occurrence probability of similar events at least 10-fold. We estimate that compared to the current climate, such events will become 10 times and 14 times more likely until the middle and end of the 21st century, respectively, under a high-emissions scenario. This increase in likelihood can be substantially reduced (to seven times more likely) under a low-emissions scenario. Our study demonstrates the effect of anthropogenic climate change on high-impact compound extreme events and highlights the urgent need to reduce greenhouse gas emissions.

1. Introduction

Compound extreme events cause impacts that are often much more severe than those of individual extreme events (Zscheischler et al., 2018, 2020). Scientific research to address whether and to what extent anthropogenic climate change has altered the characteristics of a particular extreme event—"event attribution"—has thus far focused largely on univariate extremes (Herring et al., 2022). Event attribution is a key aspect of understanding climate-change risks (Stott et al., 2016). In particular, it is vital to inform society how climate change is worsening extreme events and further guide the community to better prepare for future increases in climate-related risks and to better rebuild cities and infrastructure after disasters to be more resilient in an impending climate-changed world (Stott, 2016; Qian et al., 2022a). Concepts for the attribution of compound extreme events have only emerged recently (Chiang et al., 2021; Zscheischler and Lehner, 2022; Bevacqua et al., 2023).

Among the various types of compound extreme events, spatially compounding events occur when multiple connected locations are concurrently affected by the same or different hazards, thus inducing an aggregated impact (Zscheischler et al., 2020). Attribution studies of spatially compounding events are still rare, and limited to those considering the same hazard (Vogel et al., 2019; Verschuur et al., 2021; Zscheischler and Lehner, 2022). Attributing different types of spatially co-occurring hazards is methodologically challenging because of the different spatiotemporal scales often involved. It is a challenge, for example, to design a compound index that is impact-relevant and can easily be applied to model simulations.

The commonly used *risk-based* (or *probability-based*) *framework* for event attribution treats an observed event as one of a class of similar

* Corresponding author. Key Laboratory of Regional Climate-Environment for Temperate East Asia, Institute of Atmospheric Physics, Chinese Academy of Sciences, Beijing, China.
E-mail address: qianch@tea.ac.cn (C. Qian).

https://doi.org/10.1016/j.wace.2023.100616
Received 20 July 2023; Received in revised form 5 October 2023; Accepted 10 October 2023
Available online 11 October 2023

events and helps provide guidance for future adaptation and disaster recovery (Stott et al., 2004; Otto et al., 2016; Philip et al., 2020). However, this approach does not provide much information on the event itself. As an alternative, the *storyline framework* for event attribution examines the contribution of various factors to the specific event itself and is valuable for understanding the evolution of the event in response to various drivers (Trenberth et al., 2015; Shepherd, 2016). The storyline approach generally neglects possible changes in the configuration of the dynamics behind the event, but it is possible for the dynamic configuration to also be altered by anthropogenic forcings (Otto et al., 2016; Shepherd, 2016). The two frameworks provide complementary insights into a high-impact event (Shepherd, 2016; Qian et al., 2022a). However, they are rarely used in combination (Ye and Qian, 2021; Qian et al., 2022b).

In this paper, we develop a storyline–probability combined framework for applying extreme event attribution to spatially compounding events that involve different hazards, with the goal of increasing confidence in the attribution statement. We combine the storyline and risk-based approaches to quantify the contribution of large-scale atmospheric circulation resembling the observations of the event (dynamic effect) and anthropogenic forcings conditional on the atmospheric circulation (thermodynamic effect) to the intensity of the event and the overall anthropogenic contribution to the intensity and the occurrence probability of similar events.

We illustrate the proposed approach for a spatially compounding event that occurred in China in 2020. A record-breaking persistent heavy rainfall event struck the middle and lower reaches of the Yangtze River in China during the Meiyu period (June–July) in 2020. At the same time, South China suffered from a concurrent record-breaking heatwave event (Ye and Qian, 2021) (Fig. 1). These two events contributed to widespread severe flooding and drought, respectively, in the two regions. Both areas are important economic centres with high population densities. Attribution studies of the precipitation event alone have been carried out based on climate model simulations (Zhou et al., 2021; Lu et al., 2022; Tang et al., 2022), and these studies consistently concluded that anthropogenic forcing has reduced the occurrence probability of the extreme precipitation event in 2020 almost by half (Zhou et al., 2021; Lu et al., 2022; Tang et al., 2022). Conditional attribution of the contributions of climate change and atmospheric circulation to the precipitation and temperature events has been estimated separately, based on observational and reanalysis data (Ye and Qian, 2021). In that study, it was found that atmospheric circulation explained about 71% and 44% of the extreme precipitation event and the concurrent heatwave event, respectively; and that compared with past climate under similar atmospheric circulation conditions, the occurrence probability of an event reaching or exceeding the 2020 Meiyu amount increased by about five times under the present climate, and heatwave events reaching or exceeding a threshold of one standard deviation increased from 0.6% under past climate conditions to 69% under the present climate. Both events were driven by the same modulator, i.e. an intensified western Pacific subtropical high (Ye and Qian, 2021), and strongly affected the agricultural sector in both regions. According to statistics from the Ministry of Emergency Management, the persistent heavy rainfall in the middle and lower reaches of the Yangtze River affected approximately 3.5798 million ha of crops, including 893.9 thousand ha that experienced crop failure, resulting in direct economic losses of 132.2 billion Chinese Yuan for July alone (https://www.mem.gov.cn/xw/yjglbgzdt/202101/t20210102_376288.shtml). The inundation of crops also resulted in a phenological delay in crop growth in 2020 (Qin et al., 2022) and a reduction in vegetable yields. The heatwave in South China also affected the growth of vegetables there. As a result, the national Consumer Price Index for Vegetables in July 2020 in China saw year-on-year increases of 11.4% (https://sannong.cctv.com/2020/08/05/ARTIv08N1New9JFarvghwIqV200805.shtml). We therefore consider this event to be a spatially compounding extreme event (Zscheischler et al., 2020) and focus on a compound index that is, effectively, the average of the standardized temperature and precipitation anomalies in both regions. We conducted an event attribution analysis employing both the storyline approach (Shepherd, 2016), which is conditional on the large-scale atmospheric circulation, and the unconditional risk-based approach (Stott et al., 2004).

We first estimated the contribution of the atmospheric circulation resembling the observations in 2020 (dynamic effect) and that of anthropogenic forcings conditional on the atmospheric circulation (thermodynamic effect) to the intensity of the event from a storyline perspective to demonstrate the role of anthropogenic forcings. In the storyline approach, we propose a novel constructed flow analogues (CFA) method to evaluate the contribution of the dynamic effect. CFA can construct analogues of atmospheric circulation that are almost the same as the observed atmospheric circulation and, thus, better estimate its contribution compared to the flow analogues method (Yiou et al., 2007; Jézéquel et al., 2018), which has limitations when the intensity of the extreme event is too strong to find suitable analogues. When estimating the thermodynamic effect, we used the simulation from the latest Met Office attribution system, the HadGEM3-GA6-N216 model (Ciavarella et al., 2018), and conditioned the atmospheric circulation using the CFA method to resemble that of 2020. This storyline approach can help us better understand the compound event itself. We also took into account the possible influence of anthropogenic forcings to changes in atmospheric circulation by integrating a risk-based analysis of the intensity of similar events with the same return period based on the HadGEM3-GA6-N216 model and compared the result with that from phase 6 of the Coupled Model Intercomparison Project (CMIP6) multi-model ensembles (Eyring et al., 2016). By using CMIP6, we further estimated the role of historical emissions of greenhouse gases (GHGs) and anthropogenic aerosols (AAs).

We then carried out a risk-based attribution in terms of the probability of occurrence risk of similar compound events. This risk-based approach, which we also applied to future projections, takes into account the influences of anthropogenic forcings on the atmospheric circulation and involves the probability of similar compound events; thus, it is valuable for future adaptation.

2. Data and methods

2.1. Observational data

We used the observed daily maximum temperature (T_{max}) and 24-h precipitation data (R) for the period 1961–2020 from the CN05.1 dataset (Wu and Gao, 2013) (resolution of 0.25° × 0.25°), which was obtained based on interpolation from over 2400 observing stations in China. For atmospheric circulation data, we used the daily mean sea level pressure (SLP), surface pressure (SP), geopotential height at 500 hPa (Z500), wind, and specific humidity (eight levels, from 1000 to 300 hPa) from the NCEP–NCAR Reanalysis I dataset (Kalnay et al., 1996) with a resolution of 2.5° × 2.5° for the period 1961–2020.

2.2. Model descriptions and evaluation

Model simulations with daily resolutions from CMIP6 were used (see Supplementary Table S1 for details on model names, scenarios, and number of ensemble members). Data include historical simulation experiments with combined natural and anthropogenic forcing (Eyring et al., 2016), Detection and Attribution Model Intercomparison Project (DAMIP) experiments with individual forcing only (Gillett et al., 2016), and the Shared Socioeconomic Pathway 1–1.9 (SSP1-1.9), 2–4.5 (SSP2-4.5), and 5–8.5 (SSP5-8.5) scenario experiments for future projections (O'Neill et al., 2016). We combined historical simulations with corresponding SSP2-4.5 scenarios to extend the data to 2020 for attribution analysis.

Additionally, we used model simulations with and without anthropogenic forcings (historical and historicalNat, respectively) from the

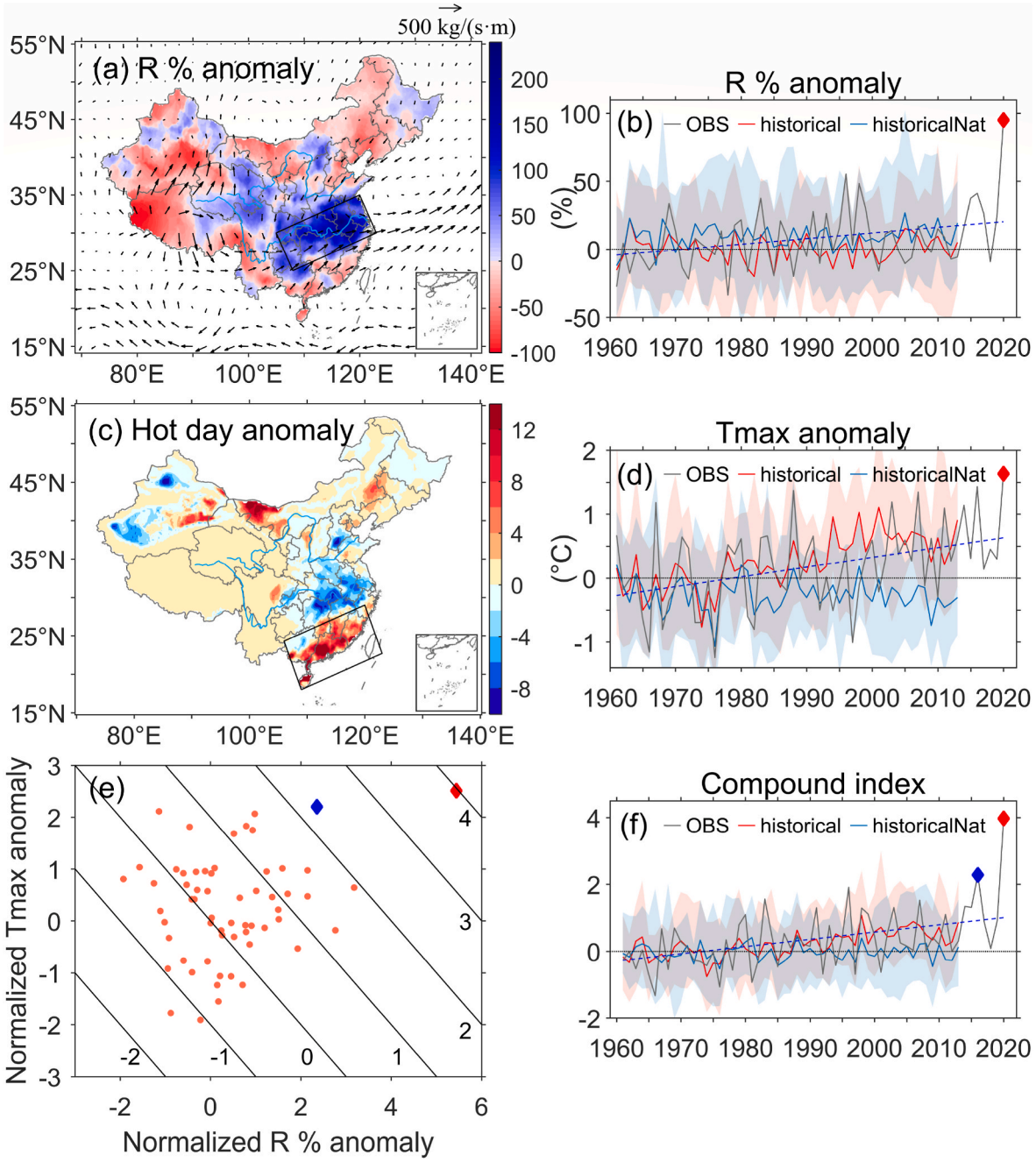

Fig. 1. Characteristics of the spatially compound event of 2020. (a) Spatial distribution of the observed precipitation anomaly in percentages (R% anomaly, shading) and the column-integrated moisture flux anomaly from 1000 to 300 hPa (vectors; kg $(s\ m)^{-1}$) during June–July 2020. (c) Anomaly in the number of hot days (days with a daily maximum temperature $T_{max} > 35$ °C) during June–July 2020. Time series of the (b) average precipitation percentage anomalies, (d) temperature anomalies, and (f) compound index over target areas (shown as the black box in (a) and (c)) based on observations (1961–2020) and the HadGEM3-GA6-N216 model ensemble means (1961–2013) under historical (red) and historicalNat (blue) experiments (shading indicates a range of 15 member simulations of the model). The blue dashed line represents the linear trend. The red diamonds in (b), (d), (e) and (f) indicate the 2020 event (in (e) and (f), the second strongest compound event that occurred in 2016 is also shown, in blue). (e) Bivariate distribution of the normalized R% anomaly and normalized T_{max} anomaly based on observational data (red dots) during 1961–2020, with isolines indicating equal levels of the compound index (Equation (1)). (For interpretation of the references to colour in this figure legend, the reader is referred to the Web version of this article.)

latest Met Office attribution system—the HadGEM3-GA6-N216 model (Ciavarella et al., 2018). This model has 525 members for 2020 for each experiment (historicalExt and historicalNatExt, respectively; hereafter, Hist2020 and HistNat2020, respectively), forced by the observed sea surface temperature/sea-ice concentration (SST/SIC) and external forcings in 2020. Such a large number of ensemble members is relevant given that a large sample size is required for robust attribution of compound events (Bevacqua et al., 2023). Fifteen members of the historical simulations for 1961–2013 were used to evaluate the model performance.

We interpolated the observed and model-simulated precipitation and temperature data to a common 1° × 1° grid. Then, we calculated the area-weighted average of the precipitation anomaly percentages (hereafter, the R% anomaly) in the middle and lower reaches of the Yangtze River (120.0°E|35.0°N, 123.0°E|30.0°N, 108.0°E|25.0°N, 105.0°E|30.0°N) and that of the T_{max} anomaly in South China (120.0°E|29.0°N,

123.0°E|22.7°N, 109.0°E|18.0°N, 106.0°E|24.3°N) over June–July (Fig. 1a–d; the two regions were delineated by Ye and Qian (2021), but we exclude grid points with land portions that are less than 50%). Following Zhang et al. (2020), we used the R% anomaly rather than the R anomaly in order to reduce the effect of the model biases on the climatological values and anomalies. In detail, we first calculated the area-weighted average of the precipitation (temperature) over June–July and then calculated its anomaly percentage (anomaly). All anomalies were calculated relative to the 1961–1990 climatology for all datasets separately. For each model, the climatology is estimated via averaging the ensemble mean of the historical simulations.

Model evaluation was divided into three parts, an approach similar to that described in Zscheischler and Lehner (2022). Firstly, we assessed whether the observed and model-simulated distributions for the T_{max} anomaly and R% anomaly were significantly different based on a Kolmogorov–Smirnoff (K–S) test. Secondly, we checked whether the observed and model-simulated empirical copula distributions between these two variables were significantly different based on a Cramér-von Mises (C-VM) test (Genest et al., 2009). Lastly, we assessed the models' skill in simulating the correlation between these two variables. All evaluations were conducted based on the period of 1961–2013 for the HadGEM3-GA6-N216 model and 1961–2014 for the CMIP6 models. The evaluation results are shown in Supplementary Table S2, and only models passing the evaluation (i.e., the HadGEM3-GA6-N216 model and four CMIP6 models) were included in the subsequent attribution and projection analyses.

2.3. Index for the spatially compounding event

In order to quantify the magnitude of the spatially compounding event, we defined a compound index:

$$Compound\ index = \frac{1}{2}\left(\frac{T_{anom}}{\sigma_{T_{anom}}} + \frac{R\%_{anom}}{\sigma_{R\%anom}}\right) \quad (1)$$

Here, T_{anom} and σ_{Tanom} represent the T_{max} anomaly and climatological standard deviation, respectively, for the area-weighted-average time series in South China (Fig. 1d). $R\%_{anom}$ and $\sigma_{R\%anom}$ are the same, but for the R% anomaly in the middle and lower reaches of the Yangtze River (Fig. 1b). Note that each term in Eq. (1) is a standardized anomaly and dimensionless quantity to allow comparability across variables (Dabernig et al., 2017). Hence, this index assumes that individual extremes in temperature and precipitation and moderate extremes in both variables at the same time are equally relevant to a potential impact. Other assumptions on the functional relationship of the compound index could be made, but without impact data to calibrate this relationship, they all seem equally valid (Bevacqua et al., 2021). It should be noted that the results obtained from the subsequent reconstructions from flow analogues for 2020 based on reanalysis data were also normalized by the observed climatological means and climatological standard deviations so that they could be compared with the observed intensity; however, the corresponding indices from model data were normalized by their own climatological means and climatological standard deviations. The standard deviation of a model was calculated as the multi-ensemble mean of the standard deviation of each ensemble member of that model.

We analysed the linear trend in the observed index and its statistical significance using the nonparametric Wang and Swail (2001) iterative method, considering repeated values in the significance testing (Qian et al., 2019). We regarded the linear trend as statistically significant using an alpha level of 5%.

2.4. Storyline analyses: dynamical and thermodynamical contribution to the intensity of the 2020 compound event

Here, we express the intensity of the extreme event as:

$$M(E) = M(D) + \mathrm{M(ND)} \quad (2)$$

where M is the magnitude of the event itself (E), D is the dynamical situation, and ND is the nondynamical situation (the complement of D). With the storyline approach, we examine the role of the various factors contributing to the event itself as it unfolded in a conditional manner (Shepherd, 2016), but with the sole focus here on large-scale atmospheric circulation and anthropogenic forcings. The first term in Eq. (2) is estimated via conditioning on atmospheric circulation conditions that resemble the D that occurred in 2020. The second term in Eq. (2) includes (i) the thermal effect of anthropogenic forcings conditioning the atmospheric circulation to resemble that of 2020, (ii) the possible influence of anthropogenic forcings on the changes in atmospheric circulation, and (iii) other effects. Here, we only focus on effect (i) and leave effect (ii) in the risk-based attribution of the intensity of similar events with the same return period. We did not consider effect (iii) in this study.

We first estimated the contribution of atmospheric circulation to the intensity of the 2020 event as the ratio of the difference between the reconstructed intensity under analogue and random atmospheric circulation patterns to the observed intensity in June–July. In order to do so, we developed a new method. Deser et al. (2016) proposed the constructed circulation analogue (CCA) approach to estimate the dynamical contribution to winter surface air temperature trends over North America during 1963–2012. We introduced this CCA method into the event attribution to estimate the contribution of atmospheric circulation and refined the CCA method to make it more appropriate for our purposes by incorporating steps from the flow analogue method. We coined this new method as the CFA approach. It involves picking out daily analogues, combining them to obtain the reconstructed value of the variable, and calculating the contribution of the atmospheric circulation to the intensity of a target event. The main steps of this CFA approach are shown in Supplementary Fig. S1. Specifically, we selected the closest Na analogues of the dynamic situation in 2020 according to the spatial pattern of atmospheric circulation for each day in June–July 2020 from a ±30-d window centred on the target day over the period 1961–2019. We then randomly subsampled Ns analogues from the Na analogues to compute their optimal linear combination that best fit the target atmospheric circulation field for each day. The coefficients of the combination were calculated based on singular value decomposition. Then, the corresponding T_{max} or R% anomalies of the Ns analogues were also combined linearly based on the same coefficients to obtain the reconstructed anomalies conditional to the observed atmospheric circulation for each day in June–July. This CFA approach can construct analogues of atmospheric circulation that are almost the same as the observed spatial patterns and thus better estimate the contribution of the atmospheric circulation to extreme events than the original flow analogue, without the cost of decreasing sample size. Note that the nonlinear trend of all variables (estimated based on quadratic polynomial fitting (Deser et al., 2016; Ye and Qian, 2021) in this study) was removed prior to selecting the analogues to minimize the impact of climate change (Deser et al., 2016; Jézéquel et al., 2018; Ye and Qian, 2021).

In this study, we determined Na = 100 and Ns = 25, according to the resultant relatively small root-mean-square error (RMSE) (Supplementary Fig. S2). After sensitivity testing (Supplementary Figs. S3 and S4), we determined that the suitable target area to calculate the flow analogue was the small-sized area (102°–123°E, 16°–35°N) (shown in Supplementary Figs. S1, S3a, and S4a), the suitable atmospheric circulation variable was SLP (Supplementary Figs. S3b and S4b), and the suitable method of measuring the similarity between atmospheric circulation patterns was the spatial Pearson correlation coefficient (Supplementary Figs. S3c and S4c). Note that the sensitivity testing in Figs. S3 and S4 was carried out after removing the trends of all variables prior to selecting the analogues, to minimize the impact of climate change as stated in the previous paragraph. The underestimations reflect the positive contribution of climate change. We reconstructed the daily T_{max} anomaly and corresponding R% anomaly simultaneously over June

and July based on the steps in Supplementary Fig. S1, and then calculated the bimonthly mean anomalies and the compound index. These steps were repeated 10,000 times (Fig. 2a).

We estimated the contribution of atmospheric circulation (dynamic effect) to the intensity of the 2020 event based on the above reconstructions from the CFA approach (Fig. 2a). We combined some steps from the flow analogues method (Yiou et al., 2007; Jézéquel et al., 2018) in calculating Control-1 and Control-M, which respectively represent totally random atmospheric circulation patterns (reconstructed completely randomly) and considering the persistence in the atmospheric circulation (reconstructed randomly, but the analogues in the adjacent *M* days were not repeatedly picked). Here, *M* represents the number of days for which the atmospheric circulation persists and is obtained from an autoregressive moving average model, as in Ye and Qian (2021). The contribution of the dynamic effect to the intensity of the event was then estimated by subtracting the median of Control-M from the median of 10,000 reconstructed results obtained from the CFA approach and then dividing the observed intensity of the event, as in Jézéquel et al. (2018).

We then estimated the contribution of the thermodynamic effect (effect of anthropogenic forcings conditional on the atmospheric circulation pattern) to the intensity of the 2020 event based on the CFA approach (Fig. 2b). We conditioned the spatial pattern of the atmospheric circulation to resemble that observed in 2020 in the Hist2020 and HistNat2020 simulations and then computed the difference between the medians of the reconstructed compound index in these two simulations divided by the observed compound index in 2020. The resultant value was regarded as the contribution of the thermodynamic effect to this compound event. One may argue that anthropogenic forcings may affect the atmospheric circulation and thus counteract or enhance the thermodynamics (Seneviratne et al., 2021); this effect is considered in the subsequent unconditional risk-based analysis.

2.5. Risk-based analyses: intensity and probability

We conducted risk-based analyses based first on intensity and then on probability for different purposes. For the intensity analysis (Fig. 2c), we estimated the contribution of the anthropogenic forcings to the intensity of the events with the same return period as that observed in 2020 to complement the results of the storyline attribution. We used the return level at the observed return period instead of the magnitude of the event as a way to account for the model-simulated bias in the magnitude. This way of accounting for model bias was also adopted by the World Weather Attribution initiative (van Oldenborgh et al., 2021). We fitted and calculated return periods of the compound index from observations and different model simulations based on the generalized extreme value (GEV) distribution, after a goodness-of-fit testing by quantile–quantile plotting (Supplementary Fig. S5). For the

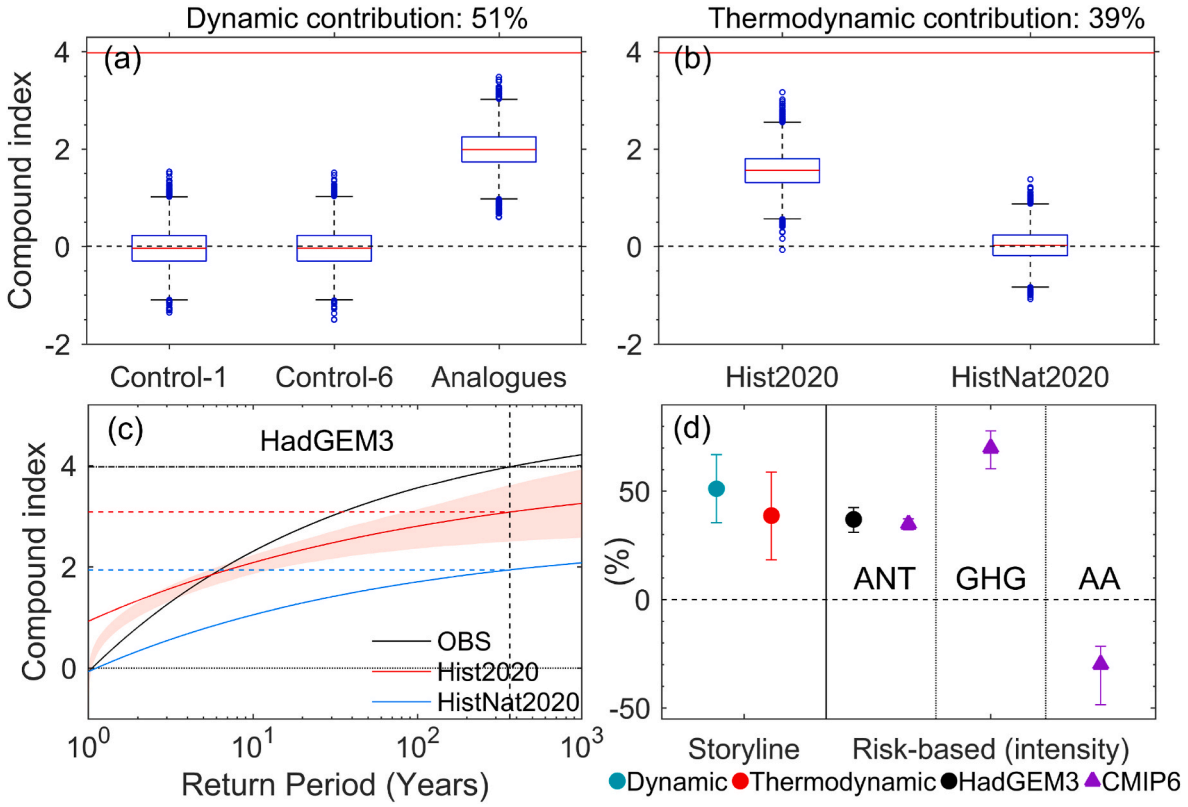

Fig. 2. The attribution results obtained from the combined approach. (a) Dynamic and (b) thermodynamic contributions to the intensity of the 2020 event based on a conditional storyline approach. (a) The reconstructed detrended compound index is based on all days (left-hand boxplot), randomly subsampled days (subsampled every six days to correct for serial dependence) (middle boxplot), and constructed flow analogues (right-hand boxplot). The red line represents the corresponding observed value in 2020. (b) Distributions of the reconstructed compound index based on HadGEM3-GA6-N216 model simulations with (Hist2020) and without (HistNat2020) anthropogenic forcings for 2020. (c) Return periods fitted using the GEV distribution based on the HadGEM3-GA6-N216 model. The dashed area indicates the 5%–95% uncertainty range obtained from 1000 subsamples with data lengths the same as those of the observations. The horizontal and vertical black dashed lines represent the observed intensity of the event and the corresponding return period, respectively. The horizontal red and blue dashed lines represent the model-simulated intensity of the events with the same return period as in the observations based on the Hist2020 and HistNat2020 simulations, respectively. (d) Dynamic and thermodynamic contributions of this event from the storyline approach conditioning the atmospheric circulation and contribution of the anthropogenic (ANT) forcings to the intensity of 2020-like events based on a risk-based approach estimated from different models. Vertical bars denote the 5%–95% uncertainty range obtained from 1000 instances of bootstrap resampling. The contribution of greenhouse gas (GHG) forcing and that of anthropogenic aerosol (AA) forcing are also shown. (For interpretation of the references to colour in this figure legend, the reader is referred to the Web version of this article.)

observations, we used a nonstationary-extremes fitting model to estimate the return period. In detail, we fitted the GEV distribution of the compound index during 1961–2020 that allowed the location (μ) and scale (σ) parameters to scale with the 4-year smoothed global mean surface temperature anomaly ($T^{'}$) (section 4.3.2 in Philip et al., 2020):

$$\mu = \mu_0 \exp\left(\frac{\alpha T^{'}}{\mu_o}\right), \sigma = \sigma_0 \exp\left(\frac{\alpha T^{'}}{\mu_o}\right) \quad (3)$$

The fit was performed using a maximum likelihood method varying $\boldsymbol{\alpha}$, μ_0, and σ_0. We then obtained the return period for the climate of 2020. For the HadGEM3-GA6-N216 model, there are simulations for 2020 that represent factual climate conditions (Hist2020) and counterfactual climate conditions (HistNat2020). For the CMIP6 models, we used historical simulations for the most recent 20 years (2001–2020) as samples representing the near-present-day climate conditions, as in Christidis and Stott (2015). Using 20 years of samples centred on the year of the event is ideal; however, hist-nat simulations ended in 2020. Since the hist-nat simulation is stationary in the long run, we used the entire period (1850–2020) as the counterfactual climate conditions, as in Christidis and Stott (2022). The intensity when the return period reached the observed one in the Hist2020 (historical in CMIP6) simulations was compared with that in the corresponding HistNat2020 (hist-nat in CMIP6) simulations (Fig. 2c), and their difference when divided by the intensity of each model's Hist2020 (historical in CMIP6) simulation was regarded as the contribution of anthropogenic forcings to the intensity of 2020-like events (Fig. 2d). Bootstrap resampling was then used to estimate the 95% confidence intervals of this contribution. It should be noted that we pooled the high-performing CMIP6 (Supplementary Table S2) multi-model ensemble simulations as though they were from one model, as has commonly been adopted in previous event attribution studies (Chiang et al., 2021; Min et al., 2022), because we did not find inconsistencies between the modelled variability of the compound index and that in the observations when assessing their standard deviations (Supplementary Fig. S6). In detail, we estimated the forced response by first averaging the individual CMIP6 model runs and then averaging all the available models. The modelled variability was estimated by the individual model simulation minus the forced response. We then compared the standard deviation of the detrended compound index in the observations with that in the modelled variability (Supplementary Fig. S6).

For probability analysis (Fig. 3), we adopted the concepts of fraction of attributable risk (FAR; Stott et al., 2004) and probability ratio (PR; Fischer and Knutti, 2015) to carry out the event attribution and future projection. FAR was defined as $-1 - P_0/P_1$, in which P_1 indicated the occurrence probability of similar events under factual climate conditions, and P_0 indicated that under counterfactual climate conditions (Stott et al., 2004). PR was defined as P_1/P_0 (Fischer and Knutti, 2015). We regarded the previous record-breaking value (in the year of 2016) as the threshold, since 2020 was the single year that exceeded the previous record (Fig. 1f), and then analysed the occurrence probability of similar events (equal to or larger than the threshold). Using this threshold allows us to examine whether the occurrence probability of experiencing a more severe year than the record-breaking 2016 (such as 2020) has

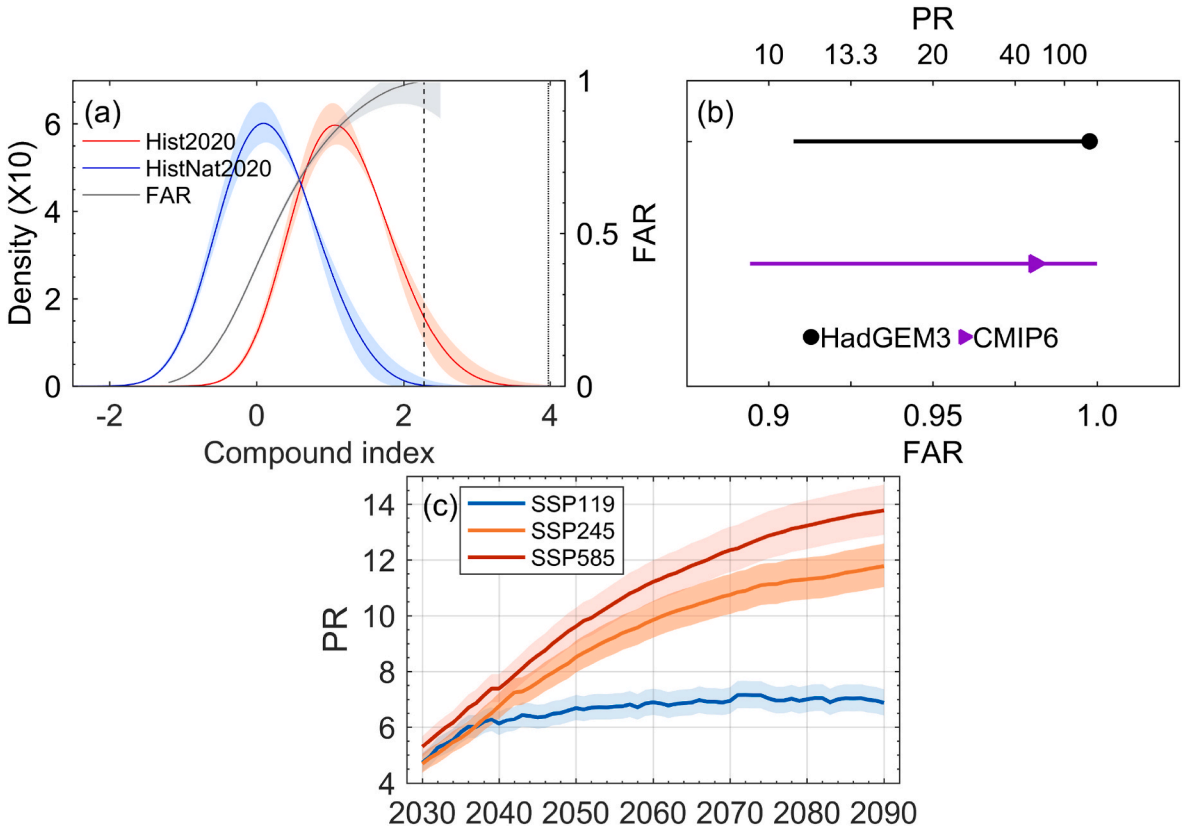

Fig. 3. Attribution and projection of the compound extreme event based on the risk-based approach. (a) GEV distributions of the compound index in the Hist2020 (red) and HistNat2020 (blue) simulations from the HadGEM3-GA6-N216 model. The dashed and solid lines represent the intensities of the 2016 and 2020 events, respectively. The grey line shows the fraction of attributable risk (FAR; see *y*-axis on the right side of the panel). (b) The FAR value (bottom axis, the corresponding probability ratio (PR) is shown on the top axis) associated with the 2020-like event based on the HadGEM3-GA6-N216 (black) and CMIP6 (purple, the multi-model ensemble is shown) models. Horizontal bars denote the 5%–95% uncertainty range (see Section 2.5). (c) The PR obtained from the GEV distributions based on three different scenarios in CMIP6 (a 20-year moving window from 2021 to 2100) compared with the near-present-day climate (historical simulations of 2001–2020). Shaded areas denote the 5%–95% uncertainty range (see Section 2.5). (For interpretation of the references to colour in this figure legend, the reader is referred to the Web version of this article.)

changed. Selection of this threshold, rather than the value in 2020, is also a way to reduce the selection bias and has commonly been used in previous event attribution studies (Stott et al., 2004; Lewis and Karoly, 2013; King et al., 2014; Knutson et al., 2014). Using the HadGEM3-GA6-N216 model, we fitted the GEV distribution to compound index values in the Hist2020 and HistNat2020 simulations and calculated the corresponding FAR/PR values to show the effect of anthropogenic forcings on the frequency of similar events (Fig. 3a and b). We also compared the results with those from the CMIP6 models, using historical simulations of 2001–2020 as near-present-day climate conditions and hist-nat simulations of 1850–2020 as the counterfactual climate conditions, as described earlier (Fig. 3b). The 95% confidence intervals of FAR/PR were calculated based on the Koopman method (Koopman, 1984). This method regards the occurrence of events as samples from a binomial distribution, which can be counted and then used to calculate test statistics (Paciorek et al., 2018; Zscheischler and Lehner, 2022).

To further explore the role of precipitation and temperature in changes in the compound index, we used the normal kernel function to construct univariate and bivariate probability density functions (Bowman and Azzalini, 1997) to demonstrate changes such as that of the R% anomaly and T_{max} anomaly in different simulations (Fig. 4).

3. Results

3.1. Observed trends in the spatially compound event

Driven by an anomalous convergence of moisture flux, the observed precipitation percentage anomaly (R% anomaly) averaged in the middle and lower reaches of the Yangtze River over June and July 2020 was record-breaking based on data going back to 1961 (Fig. 1a and b). The magnitude of the R% anomaly in 2020 reached 95%, 1.7 times the previous record in 1996, which was 56% (Fig. 1b). At the same time, South China experienced an anomalously high number of hot days, reaching up to 36 days for an individual grid box (Fig. 1c). The regional average daily maximum temperature (T_{max}) anomaly was also record-breaking (Fig. 1d). The magnitude of the T_{max} anomaly in 2020 was 1.6 °C, 1.14 times the previous record in 2016, which was 1.4 °C (Fig. 1d).

To capture the magnitude of the spatially compounding event, we employed a compound index, which is the average of the June–July normalized precipitation anomaly in the middle and lower reaches of the Yangtze River in percentages (box in Fig. 1a) and the normalized temperature anomaly in South China (box in Fig. 1c) (see Section 2.3; isolines in Fig. 1e). The compound index shows a strongly increasing trend, with a magnitude of 0.22/decade ($P = 0.00014$, section 2.3) during 1961–2020 (Fig. 1f). Its intensity in 2020 was also record-breaking, with an anomaly of four standard deviations (σ) (Fig. 1e and f). Both the T_{max} anomaly and R% anomaly in 2020 were very large (2.5σ and 5.4σ, respectively) (Fig. 1e).

3.2. Attribution of the intensity of the 2020 event

To conduct the event attribution analysis, we used climate model simulations. We evaluated the performance of the HadGEM3-GA6-N216 model and found that the historical simulations captured the temporal evolutions of the R% anomaly, T_{max} anomaly, and the compound index (Fig. 1b, d, f). Furthermore, the model represents the distribution of the R% anomaly, T_{max} anomaly, and their bivariate distribution and correlation well (Supplementary Table S2 and Section 2.2). We therefore conclude that this model can be used in the subsequent analysis.

Based on a conditional storyline approach, we quantified the dynamic and thermodynamic contributions to the intensity of the 2020 compound event (Fig. 2). To achieve this, we identified atmospheric circulation patterns that resembled the pattern of 2020, i.e., analogues, and reconstructed the compound index using our newly developed CFA method (see Section 2.4). We found that the dynamic contribution was about 51% (95% confidence intervals: 35–67%) (Fig. 2a, d), which implied that the atmospheric circulation played a significant role in the occurrence of this event. There is no trend in the temporal evolution of the number of analogues during 1961–2019 (Supplementary Fig. S7), indicating that the occurrence of the 2020 dynamic configuration is mainly controlled by the internal climate variability. Further calculation revealed that atmospheric circulation contributed 56% (35–77%) to the intensity of the R% anomaly and 41% (21–61%) to that of the T_{max} anomaly in 2020. The thermodynamic contribution was estimated to be about 39% (18–59%); this contribution was obtained via conditioning the atmospheric circulations to resemble those of 2020 in the HadGEM3-

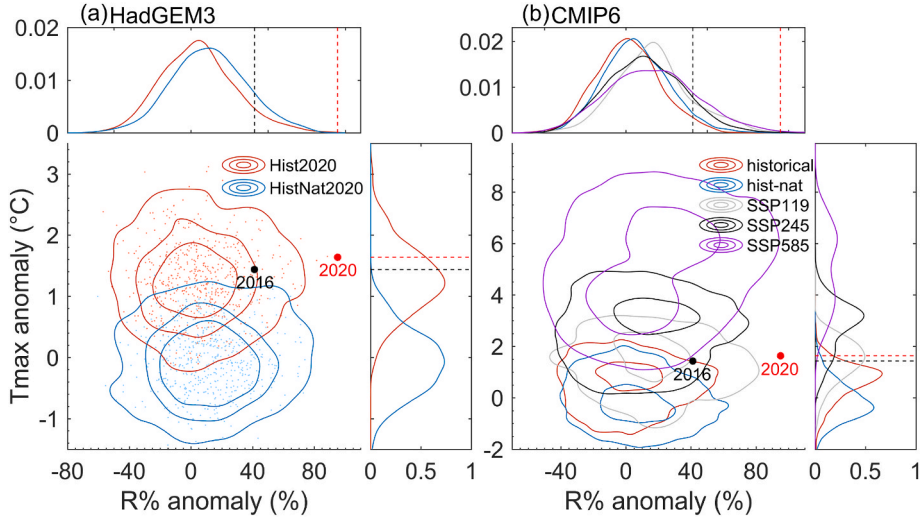

Fig. 4. Modelled changes in the univariate and bivariate distributions relevant to the event. (a) Univariate distributions of the precipitation anomaly in percentages (upper panel) and the T_{max} anomaly in °C (right panel) and their bivariate distributions (bottom left panel) based on Hist2020 (red) and HistNat2020 (blue) simulations from the HadGEM3-GA6-N216 model. The contour lines, from smallest to largest, represent 50%, 75%, and 95% of all data points. The dashed black and red lines represent the intensities of the 2016 and 2020 events, respectively. (b) The same as (a), but for the CMIP6 model based on historical (red, 2001–2020), hist-nat (blue, 1850–2020), SSP1-1.9 (grey, 2081–2100), SSP2-4.5 (black, 2081–2100), and SSP5-8.5 (purple, 2081–2100) simulations. The contour lines represent 50% and 95% of all data points. (For interpretation of the references to colour in this figure legend, the reader is referred to the Web version of this article.)

GA6-N216 model's simulations with and without anthropogenic forcings (Fig. 2b, d; see Section 2.4). This magnitude implied that the radiatively forced component also played a considerable role in the occurrence of the event.

The aforementioned thermodynamic contribution was compared with that of the overall anthropogenic forcings to the intensity of events with the same return period as the observed compound event in 2020, allowing us to consider the possible effect of anthropogenic forcings on changes in atmospheric circulation. This was conducted through a risk-based attribution that did not condition the atmospheric circulation in the HadGEM3-GA6-N216 model's simulations (Fig. 2c and see Section 2.5). We found that the overall anthropogenic contribution was about 37% (31–42%), i.e., very close to and statistically indistinguishable from the thermodynamic effect by using the storyline approach (Fig. 2d). These similar estimates of the thermodynamic and overall anthropogenic contributions indicate that the anthropogenically driven change in the frequency of the atmospheric circulation patterns is rather minor. This is also in line with the nonsignificant trends found for the occurrence of flow analogues (Supplementary Fig. S7). If we draw conclusions based on the result of the thermodynamic effect from the storyline approach alone, one may argue that anthropogenic forcings can affect atmospheric circulation too, and thus conditioning the atmospheric circulation may overestimate or underestimate the effect of anthropogenic forcings, thereby leaving the conclusion of the attribution assessment somewhat uncertain. In contrast, if we draw conclusions based on the result of the overall anthropogenic contribution from the risk-based approach alone, one may also argue that climate models may not represent the atmospheric circulation very well, and thus induce uncertainty in the contribution of anthropogenic forcings. Therefore, combining the storyline attribution approach with the risk-based attribution approach allowed us to build a complementary combined framework, thereby enhancing our confidence in the attribution statements.

To more comprehensively estimate the anthropogenic climate change effect on the event magnitude, we compared the aforementioned contribution of the anthropogenic forcings to the intensity of similar events with those from high-performing CMIP6 models (Fig. 2d; see Section 2.2, 2.5, and Supplementary Tables S1 and S2). Note that, in contrast to the HadGEM3-GA6-N216 model, the SST/SIC and radiative forcings of 2020 are not prescribed in the CMIP6 simulations. We pooled all available CMIP6 simulations, as has commonly been done in previous event attribution studies (Christidis and Stott, 2022; Min et al., 2022). This pooling of CMIP6 models can be justified because the models have variability in the compound index that is consistent with that in the observations (Supplementary Fig. S6 and Section 2.5); thus, they do not require a bias correction (Christidis and Stott, 2022). The overall anthropogenic contribution was 35% (32–37%), according to the CMIP6 multi-model ensemble. This magnitude is very close to that from the HadGEM3-GA6-N216 model (Fig. 2d). This similarity suggests only a minor influence of the SST/SIC conditions in the intensity of 2020-like events, regardless of the model differences. When we further separated the effect of the GHG forcing and AA forcing, we found that the contribution from GHG forcing was 70% (60–78%). This contribution was partly cancelled out by AA forcing, which was −30% (−49% to −22%). The magnitude of these two contributions is generally consistent among the individual CMIP6 models, except for in the MIROC6 model under ANT (anthropogenic) and AA forcings, although there are some inter-model differences (Supplementary Fig. S8a).

3.3. Attribution and projection of the likelihood of similar events

We quantified the contribution of anthropogenic forcings to the occurrence probability of 2020-like compound events based on HadGEM3-A-N216 and CMIP6 (Fig. 3a and b and Section 2.5). HadGEM3-A-N216 simulates a distribution of the compound index shifted toward higher values under historical anthropogenic forcing compared to a scenario with no emissions (Fig. 3a). Anthropogenic climate change has thus increased the likelihood of such extreme compound events. The observed intensity of the 2020 compound index in the model-simulated response to the current level of anthropogenic forcing was unprecedented, indicating how unusual the 2020 compound event was. Hence, we considered the intensity of the previous record-breaking event (2016) as the threshold by which to quantify the probability of a more intense event, such as that in 2020 (see Section 2.5 for more details). Both the T_{max} and R% anomalies were very large in 2016 (2.2σ and 2.4σ, respectively), although not as strong as those in 2020 (Fig. 1e). The FAR (Stott et al., 2004) of similar events is 0.99 (0.91, 1), equal to a PR (Fischer and Knutti, 2015) of 442.4 (10.8, Inf) based on the HadGEM3-GA6-N216 model (Fig. 3a and b). This value indicates a substantial contribution of anthropogenic forcings to the occurrence frequency of 2020-like events. The results based on the CMIP6 multi-model ensemble are similar, with a FAR of 0.98 (0.89, 1), equal to a PR of 52.6 (9.5, Inf) (Fig. 3b). The magnitude of the increase in PR is consistent among the individual CMIP6 models, except for the MIROC6 model (Supplementary Fig. S8b).

We quantified the projected occurrence probability of 2020-like compound events because of the relevance for future planning of projected changes in the frequency of extreme events under climate change. We considered a moving 20-year window from 2021 to 2100 using the CMIP6 multi-model ensembles under three typical emissions scenarios (Fig. 3c). The SSP5-8.5, SSP2-4.5, and SSP1-1.9 scenarios respectively represent a very high GHG emissions scenario, an intermediate GHG emissions scenario, and a scenario with very low GHG emissions and CO_2 emissions declining to net zero around 2060 followed by net-negative CO_2 emissions (IPCC, 2021). The SSP1-1.9 scenario will lead to global warming below 1.5 °C in 2100, in line with the Paris Agreement's 1.5 °C target. The net-zero timing in the SSP1-1.9 scenario is coincidently close to that in China's carbon neutrality scheme. We found that the future increase in the occurrence frequency of 2020-like compound events (using the value in 2016 as the threshold too) is higher in higher-emissions scenarios (Fig. 3c). Compared to near-present climate conditions (2001–2020), the event will become 10 times more frequent in 2050 and 14 times more frequent in 2090 under the SSP5-8.5 scenario; however, under the SSP1-1.9 scenario, the occurrence frequency for both years is only seven times greater (Supplementary Table S3).

To further understand the role of changes in precipitation and temperature in changes in the compound index, we explored their univariate and bivariate probability density functions estimated via the normal kernel function (Fig. 4 and Section 2.5). We found that precipitation is lower in simulations with anthropogenic forcing compared to those without anthropogenic forcing conditions in both HadGEM3-GA6-N216 (using the distribution in 2020 for reference, Fig. 4a) and the CMIP6 multi-model ensemble (using the distribution of the near-present-day climate as reference, Fig. 4b). This phenomenon is also noticeable in the time series in Fig. 1b, perhaps due to the effect of AA forcing surpassing that of GHG forcing over this stage. However, precipitation is projected to increase under future scenarios by the end of this century (Fig. 4b). The intensity of the observed 2020 precipitation event is likely an extreme value even in the SSP5-8.5 scenario (Fig. 4b), indicating the severity of the 2020 event. In contrast, temperature always tends to increase with anthropogenic forcing (Fig. 4a and b). In particular, the magnitude of the observed 2020 temperature event will be fairly normal by the end of this century under the SSP2-4.5 and SSP5-8.5 scenarios (Fig. 4b).

4. Discussion and conclusions

This paper presents a comprehensive framework for compound event attribution that combines a storyline approach with a risk-based approach to reach complementary conclusions. We refer to this approach as the storyline–probability combined approach. In the storyline approach, we also developed a novel constructed flow

analogue method to quantify the dynamic and thermodynamic contributions to the intensity of an extreme event. This approach is flexible and adaptable to other regions and other types of compound events or individual extreme events.

We found that the occurrence probability of spatially compounding events such as the record-breaking 2020 event in China, which caused quasi-simultaneous floods and extreme heatwaves over different regions of the country, was increased by anthropogenic climate change and is projected to further increase in the future. Floods and heatwaves over different regions, which may both have negative repercussions for the agricultural sector, are generally considered separately. For example, recent studies revealed that extreme rainfall reduced one-twelfth of China's rice yield over the last two decades (Fu et al., 2023), and that heat stress may cause a significant reduction of rice yield in China under future climate scenarios (Sun et al., 2022). However, the agricultural impacts of the 2020 event in China suggest that co-occurring weather hazards in different regions can compound one another and lead to aggregated national impacts. Overall, our study demonstrates the relevance of considering such spatially compounding events in attribution studies to avoid underestimating climate risks and to support the development of adaptation measures for the changing climate. Furthermore, our results suggest that controlling GHG emissions can reduce the occurrence risk of similar compound events, especially under a carbon-neutral scenario. This effect takes place through both the mitigation of warming and heavy precipitation, although the effect on the former is stronger.

Author contributions

Cheng Qian conceived the research and designed the study with Yangbo Ye, incorporating suggestions from Jakob Zscheischler and Emanuele Bevacqua; Yangbo Ye performed the analyses; Cheng Qian wrote the initial manuscript with input from Yangbo Ye; Jakob Zscheischler and Emanuele Bevacqua improved the manuscript.

Declaration of competing interest

The authors declare the following financial interests/personal relationships which may be considered as potential competing interests: Cheng Qian reports article publishing charges was provided by the National Natural Science Foundation of China.

Data availability

Data Availability is declared in the manuscript

Acknowledgments

Cheng Qian and Yangbo Ye were sponsored by the National Natural Science Foundation of China (grant no. 42341203) and the Jiangsu Collaborative Innovation Center for Climate Change. Jakob Zscheischler and Emanuele Bevacqua acknowledge the European COST Action DAMOCLES (grant no. CA17109), the Helmholtz Initiative and Networking Fund (Young Investigator Group COMPOUNDX; grant no. VH-NG-1537) and the European Union's Horizon 2020 research and innovation programme under grant no. 101003469 (XAIDA). The authors thank the two anonymous reviewers for their comments and suggestions to improve this manuscript. Cheng Qian also thanks the Climate Science for Service Partnership China (CSSP China) project, sponsored by the UK–China Research and Innovation Partnership Fund through the Met Office CSSP China as part of the Newton Fund, for providing the HadGEM3-GA6-N216 simulation data.

Appendix A. Supplementary data

Supplementary data to this article can be found online at https://doi.org/10.1016/j.wace.2023.100616.

References

Bevacqua, E., De Michele, C., Manning, C., et al., 2021. Guidelines for studying diverse types of compound weather and climate events. Earth's Future 9, e2021EF002340. https://doi.org/10.1029/2021ef002340.

Bevacqua, E., Suarez-Gutierrez, L., Jezequel, A., et al., 2023. Advancing research on compound weather and climate events via large ensemble model simulations. Nat. Commun. 14, 2145. https://doi.org/10.1038/s41467-023-37847-5.

Bowman, A.W., Azzalini, A., 1997. Applied Smoothing Techniques for Data Analysis. New York.

Chiang, F., Greve, P., Mazdiyasni, O., et al., 2021. A multivariate conditional probability ratio framework for the detection and attribution of compound climate extremes. Geophys. Res. Lett. 48 https://doi.org/10.1029/2021gl094361.

Christidis, N., Stott, P.A., 2015. Extreme rainfall in the United Kingdom during winter 2013/14: the role of atmospheric circulation and climate change. Bull. Am. Meteorol. Soc. 96, S46–S50. https://doi.org/10.1175/bams-d-15-00094.1.

Christidis, N., Stott, P.A., 2022. Anthropogenic climate change and the record-high temperature of May 2020 in western Europe. Bull. Am. Meteorol. Soc. 103, S33–S37. https://doi.org/10.1175/BAMS-D-21-0128.1.

Ciavarella, A., Christidis, N., Andrews, M., et al., 2018. Upgrade of the HadGEM3-A based attribution system to high resolution and a new validation framework for probabilistic event attribution. Weather Clim. Extrem. 20, 9–32. https://doi.org/10.1016/j.wace.2018.03.003.

Dabernig, M., Mayr, G.J., Messner, J.W., et al., 2017. Spatial ensemble post-processing with standardized anomalies. Quart. J. Roy. Meteor. Soc. 143, 909–916. https://doi.org/10.1002/qj.2975.

Deser, C., Terray, L., Phillips, A.S., 2016. Forced and internal components of winter air temperature trends over north America during the past 50 years: mechanisms and implications. J. Clim. 29, 2237–2258. https://doi.org/10.1175/jcli-d-15-0304.1.

Eyring, V., Bony, S., Meehl, G.A., et al., 2016. Overview of the coupled model intercomparison project phase 6 (CMIP6) experimental design and organization. Geosci. Model Dev. (GMD) 9, 1937–1958. https://doi.org/10.5194/gmd-9-1937-2016.

Fischer, E.M., Knutti, R., 2015. Anthropogenic contribution to global occurrence of heavy-precipitation and high-temperature extremes. Nat. Clim. Change 5, 560–564. https://doi.org/10.1038/nclimate2617.

Fu, J., Jian, Y.W., Wang, X.H., et al., 2023. Extreme rainfall reduces one-twelfth of China's rice yield over the last two decades. Nature Food 4, 416–426. https://doi.org/10.1038/s43016-023-00753-6.

Genest, C., Rémillard, B., Beaudoin, D., 2009. Goodness-of-fit tests for copulas: a review and a power study. Insur. Math. Econ. 44, 199–213. https://doi.org/10.1016/j.insmatheco.2007.10.005.

Gillett, N.P., Shiogama, H., Funke, B., et al., 2016. The detection and attribution model intercomparison project (damip v1.0) contribution to CMIP6. Geosci. Model Dev. (GMD) 9, 3685–3697. https://doi.org/10.5194/gmd-9-3685-2016.

Herring, S.C., Christidis, N., Hoell, A., et al., 2022. Explaining extreme events of 2020 from a climate perspective. Bull. Am. Meteorol. Soc. 103, S1–S129. https://doi.org/10.1175/BAMS-ExplainingExtremeEvents2020.1.

IPCC, 2021. In: Zhai, V.P., Pirani, A., et al. (Eds.), Summary for Policymakers. Climate Change 2021: the Physical Science Basis. Contribution of Working Group I to the Sixth Assessment Report of the Intergovernmental Panel on Climate Change, Masson-Delmotte. Cambridge University Press.

Jézéquel, A., Yiou, P., Radanovics, S., 2018. Role of circulation in European heatwaves using flow analogues. Clim. Dynam. 50, 1145–1159. https://doi.org/10.1007/s00382-017-3667-0.

Kalnay, E., Kanamitsu, M., Kistler, R., et al., 1996. The ncep/ncar 40-year reanalysis project. Bull. Am. Meteorol. Soc. 77, 437–471. https://doi.org/10.1175/1520-0477(1996)077<0437:Tnyrp>2.0.Co;2.

King, A.D., Karoly, D.J., Donat, M.G., et al., 2014. Climate change turns Australia's 2013 big dry into a year of record-breaking heat. Bull. Am. Meteorol. Soc. 95, S41–S45.

Knutson, T.R., Zeng, F.R., Wittenberg, A.T., 2014. Seasonal and annual mean precipitation extremes occurring during 2013: a U.S. Focused analysis. Bull. Am. Meteorol. Soc. 95, S19–S23.

Koopman, P.A.R., 1984. Confidence intervals for the ratio of two binomial proportions. Biometrics 40, 513–517. https://doi.org/10.2307/253.

Lewis, S.C., Karoly, D.J., 2013. Anthropogenic contributions to Australia's record summer temperatures of 2013. Geophys. Res. Lett. 40, 3705–3709. https://doi.org/10.1002/grl.50673.

Lu, C., Sun, Y., Zhang, X., 2022. The 2020 record-breaking mei-yu in the Yangtze River valley of China: the role of anthropogenic forcing and atmospheric circulation. Bull. Am. Meteorol. Soc. 103, S98–S104. https://doi.org/10.1175/BAMS-D-21-0161.1.

Min, S.-K., Jo, S.-Y., Seong, M.-G., et al., 2022. Human contribution to the 2020 summer successive hot-wet extremes in South Korea. Bull. Am. Meteorol. Soc. 103, S90–S97. https://doi.org/10.1175/BAMS-D-21-0144.1.

O'Neill, B.C., Tebaldi, C., van Vuuren, D.P., et al., 2016. The scenario model intercomparison project (scenariomip) for CMIP6. Geosci. Model Dev. (GMD) 9, 3461–3482. https://doi.org/10.5194/gmd-9-3461-2016.

Otto, F.E.L., van Oldenborgh, G.J., Eden, J., et al., 2016. The attribution question. Nat. Clim. Change 6, 813–816. https://doi.org/10.1038/nclimate3089.

Paciorek, C.J., Stone, D.A., Wehner, M.F., 2018. Quantifying statistical uncertainty in the attribution of human influence on severe weather. Weather Clim. Extrem. 20, 69–80. https://doi.org/10.1016/j.wace.2018.01.002.

Philip, S., Kew, S., van Oldenborgh, G.J., et al., 2020. A protocol for probabilistic extreme event attribution analyses. Adv. Stat. Climatol. Meteorol. Oceanogr. 6, 177–203. https://doi.org/10.5194/ascmo-6-177-2020.

Qian, C., Zhang, X.B., Li, Z., 2019. Linear trends in temperature extremes in China, with an emphasis on non-Gaussian and serially dependent characteristics. Clim. Dynam. 53, 533–550. https://doi.org/10.1007/s00382-018-4600-x.

Qian, C., Ye, Y.B., Chen, Y., et al., 2022a. An updated review of event attribution approaches. J. Meteorol. Res. 36, 227–238. https://doi.org/10.1007/s13351-022-1192-5.

Qian, C., Ye, Y.B., Zhang, W.X., et al., 2022b. Heavy rainfall event in mid-August 2020 in southwestern China: contribution of anthropogenic forcings and atmospheric circulation. Bull. Am. Meteorol. Soc. 103, S111–S117. https://doi.org/10.1175/bams-d-21-0233.1.

Qin, X.L., Shi, Q., Wang, D.Z., et al., 2022. Inundation impact on croplands of 2020 flood event in three provinces of China. IEEE J. Sel. Top. Appl. Earth Obs. Rem. Sens. 15, 3179–3189. https://doi.org/10.1109/jstars.2022.3161320.

Seneviratne, S.I., Zhang, X., Adnan, M., et al., 2021. In: Zhai, V.P., Pirani, A., et al. (Eds.), Climate Change 2021: the Physical Science Basis. Contribution of Working Group I to the Sixth Assessment Report of the Intergovernmental Panel on Climate Change, Masson-Delmotte. Cambridge University Press, p. 1611.

Shepherd, T.G., 2016. A common framework for approaches to extreme event attribution. Curr. Clim. Change Rep. 2, 28–38. https://doi.org/10.1007/s40641-016-0033-y.

Stott, P.A., Stone, D.A., Allen, M.R., 2004. Human contribution to the European heatwave of 2003. Nature 432, 610–614. https://doi.org/10.1038/nature03089.

Stott, P.A., 2016. How climate change affects extreme weather events research can increasingly determine the contribution of climate change to extreme events such as droughts. Science 352, 1517–1518. https://doi.org/10.1126/science.aaf7271.

Stott, P.A., Christidis, N., Otto, F.E.L., et al., 2016. Attribution of extreme weather and climate-related events. WIRES Clim. Chang. 7, 23–41. https://doi.org/10.1002/wcc.380.

Sun, Q., Zhao, Y.X., Zhang, Y., et al., 2022. Heat stress may cause a significant reduction of rice yield in China under future climate scenarios. Sci. Total Environ. 818 https://doi.org/10.1016/j.scitotenv.2021.151746.

Tang, H., Wang, Z., Tang, B., et al., 2022. Reduced probability of 2020 June July persistent heavy mei-yu rainfall event in the Middle to Lower Reaches of the Yangtze River basin under anthropogenic forcing. Bull. Am. Meteorol. Soc. 103, S83–S89. https://doi.org/10.1175/bams-d-21-0167.1.

Trenberth, K.E., Fasullo, J.T., Shepherd, T.G., 2015. Attribution of climate extreme events. Nat. Clim. Change 5, 725–730. https://doi.org/10.1038/nclimate2657.

van Oldenborgh, G.J., van der Wiel, K., Kew, S., et al., 2021. Pathways and pitfalls in extreme event attribution. Clim. Change 166, 13. https://doi.org/10.1007/s10584-021-03071-7.

Verschuur, J., Li, S.H., Wolski, P., et al., 2021. Climate change as a driver of food insecurity in the 2007 Lesotho-south africa drought. Sci. Rep. 11 https://doi.org/10.1038/s41598-021-83375-x.

Vogel, M.M., Zscheischler, J., Wartenburger, R., et al., 2019. Concurrent 2018 hot extremes across Northern Hemisphere due to human-induced climate change. Earth's Future 7, 692–703. https://doi.org/10.1029/2019EF001189.

Wang, X.L., Swail, V.R., 2001. Changes of extreme wave heights in Northern Hemisphere oceans and related atmospheric circulation regimes. J. Clim. 14, 2204–2221. https://doi.org/10.1175/1520-0442(2001)014<2204:Coewhi>2.0.Co;2.

Wu, J., Gao, X.-J., 2013. A gridded daily observation dataset over China region and comparison with the other datasets. in Chinese Chin. J. Geophys. 56, 1102–1111. https://doi.org/10.6038/cjg20130406.

Ye, Y., Qian, C., 2021. Conditional attribution of climate change and atmospheric circulation contributing to the record-breaking precipitation and temperature event of summer 2020 in southern China. Environ. Res. Lett. 16, 044058 https://doi.org/10.1088/1748-9326/abeeaf.

Yiou, P., Vautard, R., Naveau, P., et al., 2007. Inconsistency between atmospheric dynamics and temperatures during the exceptional 2006/2007 fall/winter and recent warming in Europe. Geophys. Res. Lett. 34, 52–94. https://doi.org/10.1029/2007gl031981.

Zhang, W., Li, W., Zhu, L., et al., 2020. Anthropogenic influence on 2018 summer persistent heavy rainfall in central western China. Bull. Am. Meteorol. Soc. 101, S65–S70. https://doi.org/10.1175/bams-d-19-0147.1.

Zhou, T., Ren, L., Zhang, W., 2021. Anthropogenic influence on extreme meiyu rainfall in 2020 and its future risk. Sci. China Earth Sci. 64, 1633–1644. https://doi.org/10.1007/s11430-020-9771-8.

Zscheischler, J., Westra, S., van den Hurk, B., et al., 2018. Future climate risk from compound events. Nat. Clim. Change 8, 469–477. https://doi.org/10.1038/s41558-018-0156-3.

Zscheischler, J., Martius, O., Westra, S., et al., 2020. A typology of compound weather and climate events. Nat. Rev. Earth Environ. 1, 333–347. https://doi.org/10.1038/s43017-020-0060-z.

Zscheischler, J., Lehner, F., 2022. Attributing compound events to anthropogenic climate change. Bull. Am. Meteorol. Soc. 103, E936–E953. https://doi.org/10.1175/bams-d-21-0116.1.